

A Single Stage Photovoltaic Solar Pumping System based on the Three Phase Multilevel Inverter

Ayoub Nouaiti

Laboratory of Computer Science, Applied Math and Electrical Engineering (IMAGE), EST, Moulay Ismail University of Meknes, Morocco
nouayoub@gmail.com (corresponding author)

Moussa Reddak

Laboratory of Materials, Processes, Environment and Quality, ENSA Safi, Cadi Ayyad University of Marrakech, Morocco
mreddak@uca.ac.ma

Chaymaa Boutahiri

Laboratory of Computer Science, Applied Math and Electrical Engineering (IMAGE), EST, Moulay Ismail University of Meknes, Morocco
chaymaaboutahiri@gmail.com

Abdelouahed Mesbahi

Laboratory of Energy and Electrical Systems (LESE), ENSEM, Hassan II University of Casablanca, Morocco
abdelouahed.mesbahi@gmail.com

Abdallah Marhraoui Hsaini

Laboratory of Computer Science, Applied Math and Electrical Engineering (IMAGE), EST, Moulay Ismail University of Meknes, Morocco
mhabdallah@gmx.fr

Aziz Bouazi

Laboratory of Computer Science, Applied Math and Electrical Engineering (IMAGE), EST, Moulay Ismail University of Meknes, Morocco
a.bouazi@gmx.fr

Received: 16 September 2023 | Revised: 30 September 2023 | Accepted: 16 October 2023

Licensed under a CC-BY 4.0 license | Copyright (c) by the authors | DOI: <https://doi.org/10.48084/etasr.6403>

ABSTRACT

This paper presents a study of a single-stage DC-AC converter for a solar water pumping application. The topology was based on solar panels connected to a new structure of a three-phase multilevel inverter through DC-bus capacitors. The inverter offers simplicity, requires fewer components compared to conventional ones, and provides optimal voltage and current waveforms with reduced harmonics, eliminating the need for filters. The applied control technique aimed to stabilize the input DC-bus voltage, extract the maximum power using a simple MPPT algorithm, and enhance the efficiency of the water pump through scalar V/f control, regardless of weather changes. A simulation was conducted using the PSIM software, considering a variable daily climate scenario. The results obtained demonstrate the efficiency of the system in extracting energy with optimal torque and current for the pump compared to a classic design based on a three-phase H-bridge inverter.

Keywords-photovoltaic energy conversion system; three-phase multilevel inverter; maximum power point tracking (MPPT); scalar V/f control; induction motor

I. INTRODUCTION

Access to clean water is essential for life. People extract water for their personal and livestock needs, irrigation, and various other purposes [1]. Water pumps facilitate the movement of water through pipes, tanks, or treatment facilities, using several technologies such as centrifugal, volumetric, and helical pumps [2-4]. Solar panels generate DC voltages to drive permanent magnet DC motors coupled to the pump shaft or can be converted to single or three-phase AC through inverters [5-8]. For the latter, multilevel topologies with suitable controls mitigate the problems of handling high input DC-bus voltage and power quality. Such topologies achieve low Total Harmonic Distortion (THD), reduce voltage stress (dv/dt), minimize electromagnetic interference, and require compact filter sizes [9-10].

The design of solar inverters emphasizes various parameters, including the extraction of maximum power from solar panels (MPPT techniques) [11-12], the use of battery energy storage [13], and the implementation of digital control circuits to apply efficient control algorithms [14]. Water pump three-phase induction motors are used in a wide variety of applications, which require variable power and specific water flow rates. To achieve this, several control techniques are combined with MPPT, including scalar V/f control, Field-Oriented Control (FOC) strategy, and Direct Torque Control (DTC) [15-17]. Thus, closed-loop speed control improves the performance and efficiency of the system. This study investigated a battery-less solar inverter that drove a water pump using a new structure of a three-phase multilevel inverter [18], which was constructed with a three-phase H-Bridge inverter and auxiliary power switches. Gate pulses were obtained using a conventional modulation technique, and an MPPT algorithm combined with the scalar V/f technique, controlled the system. The topology was simulated in PSIM software and analyzed with a variable climate scenario to verify the robustness of the control and the performance of the proposed inverter.

II. THE STUDIED PHOTOVOLTAIC SYSTEM

Figure 1 shows the platform of the proposed single-stage system. The principal components include photovoltaic (PV) panels and a three-phase DC-AC Multilevel Voltage Source Converter (MVSC) to supply a water pump.

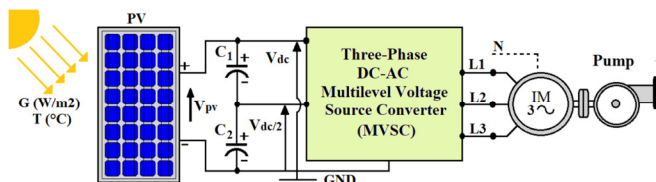


Fig. 1. The proposed single-stage system.

A. Photovoltaic Solar Panels

Different solar cells are used to manufacture solar panels, such as crystalline, amorphous, and thin-film cells. To achieve a rated power, several cells are interconnected in series/parallel configurations to create PV modules and arrays. The generated DC is obtained through the photovoltaic effect by absorbing photons from sunlight. Figure 2 shows the model of a solar cell, which consists of a current source, a single diode, a series resistance R_s , and a parallel resistance R_p [19].

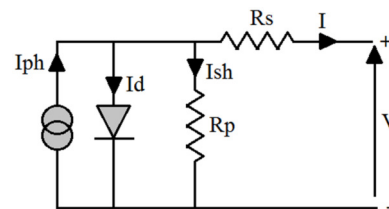


Fig. 2. Model of a solar cell.

Equation (1) expresses the produced current I from the solar cell. I_{ph} is the photocurrent, I_0 is the diode reverse saturation current, V represents the output voltage, N signifies the ideality factor of the diode, q corresponds to the charge of an electron ($1.60217662 \times 10^{-19}$ C), K stands for the Boltzmann constant ($1.38064852 \times 10^{-23}$ m²kg⁻²K⁻¹), and T denotes the junction temperature. Table I shows the electrical parameters of the adopted PV under Standard Test Conditions (STC), defined as 1000W/m² and 25°C.

$$I = I_{ph} - I_d - I_{sh} = I_{ph} - I_0 \left[\exp \left(q \cdot \left(\frac{V + (R_s \cdot I)}{n \cdot K \cdot T} \right) \right) - 1 \right] - \frac{V + (R_s \cdot I)}{R_p} \quad (1)$$

TABLE I. ELECTRICAL PARAMETERS OF THE USED PV UNDER STC

| Parameters | Values |
|------------------------------------|--------|
| Nominal power (P_{max}) | 90 W |
| Nominal Voltage (V_{mpp}) | 19.2 V |
| Nominal Current (I_{mpp}) | 4.69 A |
| Short-circuit current (I_{sc}) | 4.98 A |
| Open-circuit voltage (V_{oc}) | 23.44V |

B. Three Phase Multilevel Voltage Source Converter

The V_{PV} output voltage from the PV panels is converted into AC using the MVSC from the PV panels is converted into AC using the MVSC to provide electric power to the water pump. Figure 3 illustrates the topology of the used converter with 5 levels (MVSC-5L), which is based on [18]. The MVSC-5L is equipped with 6 switches (SAH, SAL, SBH, SBL, SCH, SCL) arranged in an H-bridge configuration, with no connection to the high-side drain terminals. Three sets of parallel power switches [(Q1, Q2), (Q3, Q4), and (Q5, Q6)] are connected to the high side of the bridge through the power switches (SAH, SBH, SCH), and a capacitor block functions as a voltage source. Figure 4 illustrates the optimal waveform shape of the AC voltages per line with the active switches.

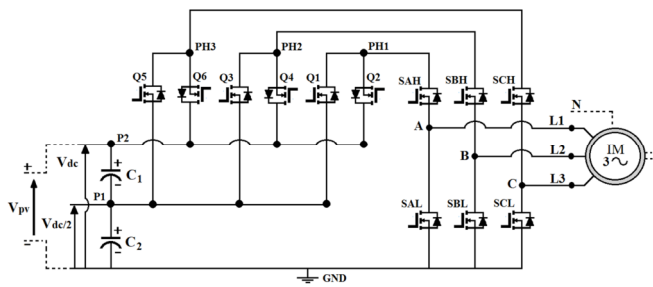


Fig. 3. The used MVSC-5L.

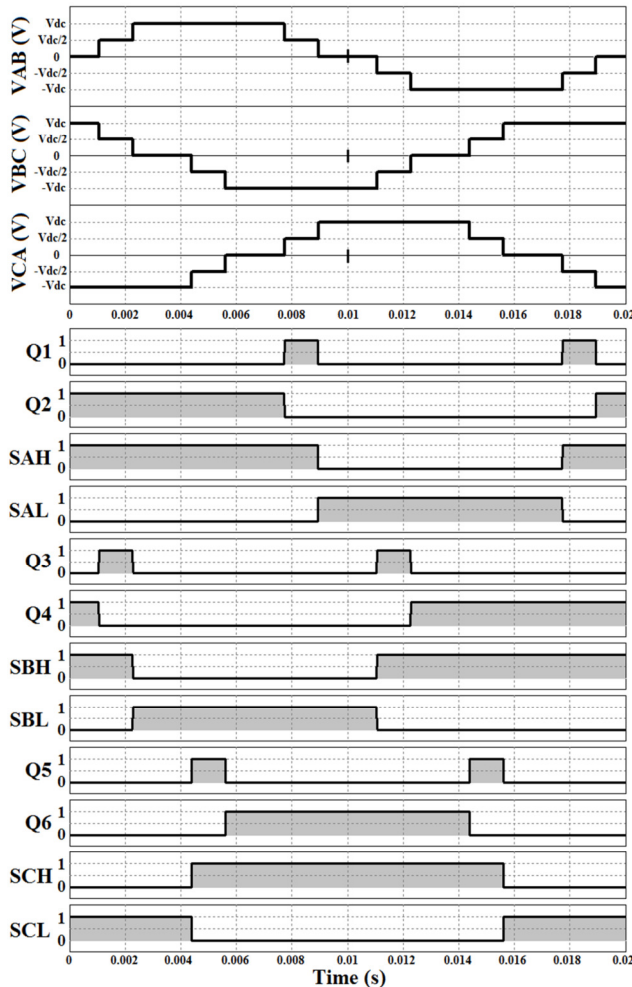


Fig. 4. Optimal waveform shape of the AC voltages per line with the active switches ($f = 50$ Hz).

Sinusoidal Pulse Width Modulation (SPWM) was used to generate the gating signals for the MVSC-5L switches. This was achieved by comparing two triangular carrier waves (Carr 1 and Carr 2) with a reference sinusoidal signal (Ref), as shown in Figure 5 and explained in Table II. The latter establishes the criteria for controlling the switches [Q1, Q2, SAH, and SAL]. As for the remaining switches ([Q3, Q4, SBH, SBL], and [Q5, Q6, SCH, SCL]), their gate pulses are generated by phase-shifting the reference signal by 120° and -120° . The modulation index (m) of the SPWM is defined as the ratio of

the peak magnitudes of the reference and the carrier waves. The MVSC-5L generates AC voltages with 5 levels per line, reducing the THD of the delivered current without the need for filters.

TABLE II. LOGICAL CONDITIONS TO ACTIVE THE POWER SWITCHES FOR ONE LEG OF THE MVSC-5L

| Signals/Conditions | ON switch |
|--|-----------|
| $(Ref \geq Carr1) = C1$ | SAH |
| $(Ref \geq Carr2) = C2$ | Q2 |
| $\{C1 \text{ AND } (\text{NOT } C2)\}$ | Q1 |
| $(\text{NOT } C1)$ | SAL |

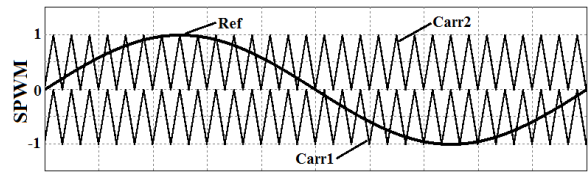


Fig. 5. SPWM technique for one leg of the MVSC-5L.

C. AC Water Pump

For the centrifugal pump, the load torque T_L is proportional to the square of the Induction Motor (IM) rotor speed Ω , as shown in (2), where K_{pump} is the constant of the pump used. T_L is equal to the torque of the induction motor T_{IM} under steady-state operation [15]. For this, T_L and nominal power P_n of the IM can be expressed as:

$$T_L = T_{IM} = K_{pump} \cdot \Omega^2 \tag{2}$$

$$P_n = K_{pump} \cdot \Omega^3 \tag{3}$$

Table III lists the parameters of the used IM with the pump [20].

TABLE III. PARAMETERS OF THE IM WITH THE PUMP

| Parameters | Values |
|-----------------------------|---------------------------------|
| Nominal power (P_n) | 1.5 Kw |
| Input power (P_a) | Around 2 KW |
| Speed (N_n) / frequency | 1400 Rpm / 50 Hz |
| Pole pairs (P) | 2 |
| Voltage (V_n) | $\Delta 220$ V / $\Delta 380$ V |
| Current (I_n) | $\Delta 6$ A / $\Delta 3.5$ A |
| K_{pump} | 47.6×10^{-5} |

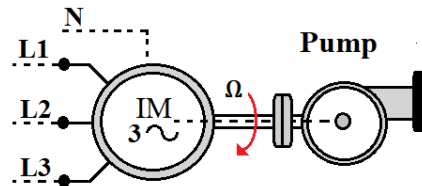


Fig. 6. IM coupled to a centrifugal pump.

III. SIZING OF DC-BUS ELEMENTS

The input DC-bus voltage (V_{dc}) and the capacitors of the MVSC-5L are determined based on the nominal parameters of the IM and the PV array.

A. DC-Bus Voltage

Equation (4) shows the expression that determines the minimum value of V_{dc} , where V_{L-L} is the line voltage across the IM terminals:

$$V_{dc-min} = \sqrt{2} \cdot V_{L-L} \tag{4}$$

Considering the IM voltage to be 380 V (star connected), the range of V_{dc} must be greater than 537 V. According to Table I, the power from the selected PV array must exceed the input power (P_a) of the IM. To achieve this, the system was designed with 31 PV connected in series. As a result, the total rating was 2.79 KW, which was higher than P_a . Therefore, the obtained V_{mpp} was 595 V, which was the selected V_{dc} reference. This was confirmed, as V_{mpp} and I_{mpp} reach approximately 80% and 90% of V_{oc} and I_{sc} , respectively [18].

B. DC-Bus Capacitors

The DC-bus capacitors provide energy stability during transients, such as a decrease in irradiance, temperature, and load. Their values are determined using [16]:

$$\frac{1}{2} C_{dc} (V_{dc}^2 - V_{dc1}^2) = 3\alpha t V_p I_p \tag{5}$$

where V_{dc} is the DC-bus voltage (595 V), V_{dc1} is the minimum voltage during the transient (575 V), α is an overloading factor (1.3), and t is the duration of the transient (0.005 s). I_p is the IM phase current (3.5 A), and V_p is the phase voltage (220 V). Thus, the calculated value was approximately 1000 μ F.

IV. CONTROL OF THE PV SYSTEM

Figure 7 shows the applied control for the single-stage PV system. The objective was to extract the maximum power from the PV array and drive the pump with optimal torque through V/f control of the IM.

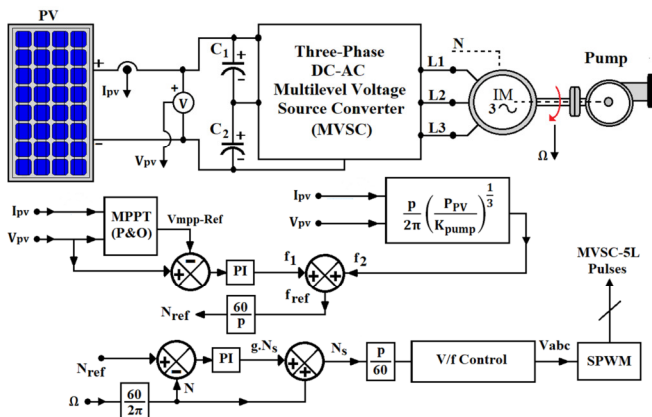


Fig. 7. PV system with the adopted control.

A. MPPT and Power Control Blocks

The voltage V_{pv} and current I_{pv} were measured and fed into the Perturb and Observe (P&O) MPPT algorithm block shown in Figure 8.

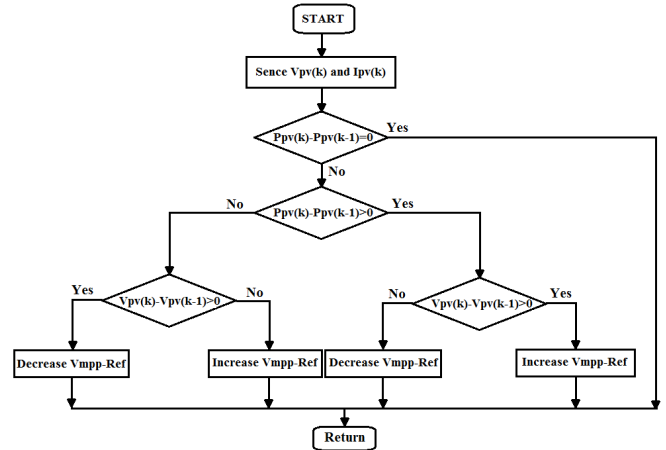


Fig. 8. Flowchart of the P&O MPPT method.

By perturbing V_{pv} , the reference voltage $V_{mpp-Ref}$ was adjusted to 595V (V_{dc}) using a PI controller. The resulting signal was the reference frequency f_1 . Based on the pump characteristics, as described in (3) and approximated in [21], a frequency f_2 was derived from the power of the PV array. The reference speed N_{ref} of the rotor was calculated using (6), where p represents the pole pairs of the induction motor.

$$N_{ref} = \frac{f_{ref} \times 60}{p} = \frac{(f_1 + f_2) \times 60}{p} \tag{6}$$

B. Speed and Scalar V/f Control Blocks

The speed (N) of the IM was sensed and compared with the calculated N_{ref} . The PI controller adjusted the error and produced the signal gN_s . Subsequently, the synchronous speed N_s was determined according to (7), where g represents the slip.

$$N_s = gN_s + N \tag{7}$$

The synchronous frequency f_s was input into the V/f block. A linear profile was established for rated values of 380V/50Hz. To achieve this, the line voltage was proportional to the frequency ($V_{L-L} \propto f$), as shown in Figure 9 [22]. The gating pulses for the MVSC-5L were then generated using the SPWM technique.

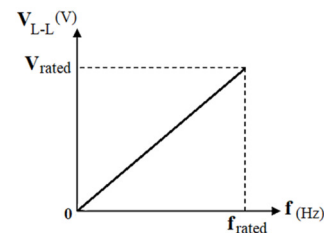


Fig. 9. Linear V/f profile.

V. SIMULATION RESULTS

The studied PV system was simulated on PSIM Software and assessed with variable irradiance and temperature levels, resembling a typical daily climate scenario, as shown in Figure 10. The profiles ranged from 257 to 922 W/m² and from 23 to 25°C, while the carrier signal frequency was set to 4 KHz.

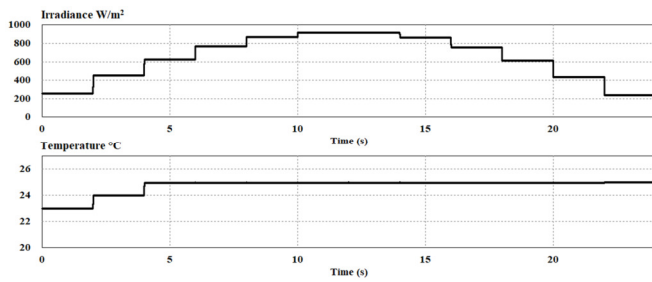


Fig. 10. Irradiance and temperature profiles.

Figures 11-13 show the results obtained during the chosen scenario, and Table IV provides a comparison of the current THD and torque of the PV system between the MVSC-5L and a conventional three-phase H-bridge inverter (VSC) [23]. Figure 11 shows that the DC-bus voltage is adjusted to the desired value (595 V) by the MPPT block controller. The current from the PV array reaches its maximum in the range of [1.15 – 4.32 A] with each variation. Consequently, the power generated by the PV array ($V_{pv} \times I_{pv}$) matches the optimal power P_{Vopt} . Figure 12 shows that the rotor speed N follows the reference speed N_{ref} within the range of 1020 - 1560 rpm. Consequently, the derived frequency f_{sin} for the SPWM varies between 35.5 and 57.5 Hz.

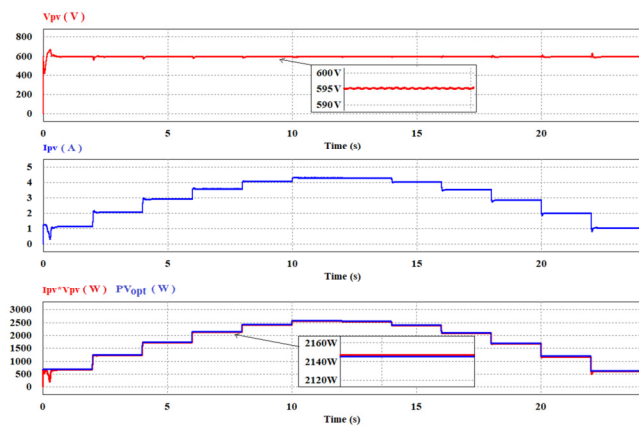


Fig. 11. PV side results: V_{pv} (V), I_{pv} (A), and Power (W).

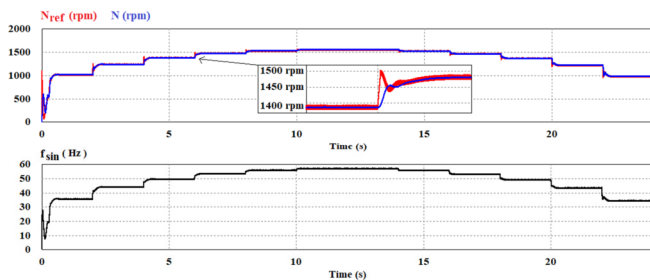


Fig. 12. Control side results: N_{ref} (rpm), N (rpm), and f_{sin} (Hz).

Figure 13 shows that the AC voltages in the IM exhibit five levels per line (U_{AB}) and nine levels per phase (V_{An}) with variable frequency and RMS values. The line voltage varies between 279 and 410 V. AC currents have a sinusoidal shape with variable RMS values in the interval of 2.37 - 4.56 A. The

torque T_L varies according to the rotor speed from 5.4 to 12.7 N.m, which validates the main achievement of the applied control. During the time interval from 4 to 6 s, f_{sin} is equal to 49.6 Hz, the rotor speed is 1387 rpm, and the RMS values of line voltage and current are 379 V and 3.53 A, respectively. This result confirms the operation of the IM under nominal conditions.

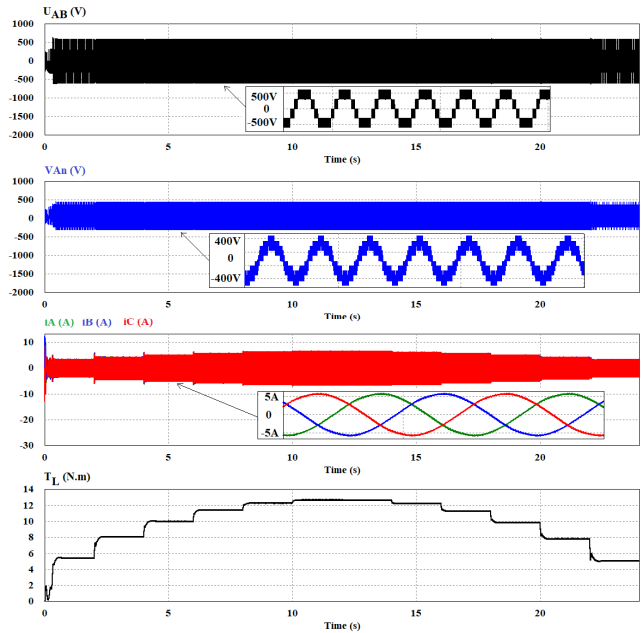


Fig. 13. Motor side results: U_{AB} (V), V_{An} (A), i_a , i_b , and i_c (A), and T_L (N.m).

TABLE IV. PERFORMANCE COMPARISON OF THE MVSC-5V WITH THE CONVENTIONAL VSC

| Irradiance (W/m ²) | MVSC-5L | | Classic VSC | |
|--------------------------------|-------------|------------------|-------------|------------------|
| | T_L (N.m) | THD of i_A (%) | T_L (N.m) | THD of i_A (%) |
| 257 | 5.41 | 1.67 | 5.45 | 5.46 |
| 453 | 8.00 | 1.38 | 8.00 | 2.48 |
| 629 | 10.00 | 1.38 | 10.00 | 2.32 |
| 771 | 11.42 | 1.59 | 11.40 | 2.31 |
| 871 | 12.29 | 2.03 | 12.27 | 2.69 |
| 922 | 12.70 | 2.18 | 12.68 | 2.65 |

From Table IV, it is evident that the studied PV system exhibits better performance in terms of torque and current THD compared to the basic VSC. The system effectively tracks the maximum power from solar panels, stabilizes the DC-bus voltage, and provides mechanical and electrical energy to the pump regardless of climate conditions. This results in improved water flow, reduced machine losses, and a positive overall impact on system performance. Compared to the control methods in [24-25], the results are notable and affirm the benefits and advantages of using multilevel inverters in PV pumping systems.

VI. CONCLUSION

This paper introduced the structure of a single-stage three-phase multilevel inverter for a PV pumping system, using a

new topology with a minimal number of switches and a straightforward modulation technique. An MPPT algorithm was applied using the scalar V/f method, and a comprehensive description of the control strategy was provided. A variable climate scenario was evaluated with the PV system, and its performance was analyzed through simulation. The topology studied demonstrated its ability to track maximum power using the P&O method, regulate input voltage, and provide the water pump motor with optimal power flow. In the five-level version, both the THD of currents and torque performance outperformed the conventional structure. This topology can be considered an attractive solution for pumping systems that combines both performance and cost-effectiveness. In future work, the proposed system will be further developed by testing other control strategies, with the possibility of implementing a hardware setup.

REFERENCES

- [1] N. Ntshako, E. D. Markus, M. Masinde, and A. M. Abu-Mahfouz, "Potable Water Quality Monitoring: A Survey of Intelligent Techniques," in *2019 International Multidisciplinary Information Technology and Engineering Conference (IMITEC)*, Vanderbijlpark, South Africa, Aug. 2019, pp. 1–6, <https://doi.org/10.1109/IMITEC45504.2019.9015868>.
- [2] A. Lipej, "Challenges in the Numerical Analysis of Centrifugal Pumps: Energetic, Cavitation and Dynamic Characteristics," *Engineering, Technology & Applied Science Research*, vol. 12, no. 1, pp. 8217–8222, Feb. 2022, <https://doi.org/10.48084/etasr.4647>.
- [3] M. M. S. (Prisecaru) and N. Băran, "Rotating Volumetric Pump for Wastewater Conveyance," *Asian Journal of Applied Science and Technology*, vol. 3, no. 4, pp. 194–198, Jan. 2020.
- [4] R. Foster and A. Cota, "Solar Water Pumping Advances and Comparative Economics," *Energy Procedia*, vol. 57, pp. 1431–1436, Jan. 2014, <https://doi.org/10.1016/j.egypro.2014.10.134>.
- [5] A. M. Kassem, "MPPT control design and performance improvements of a PV generator powered DC motor-pump system based on artificial neural networks," *International Journal of Electrical Power & Energy Systems*, vol. 43, no. 1, pp. 90–98, Dec. 2012, <https://doi.org/10.1016/j.ijepes.2012.04.047>.
- [6] S. Rahman *et al.*, "Design and Implementation of Cascaded Multilevel qZSI Powered Single-Phase Induction Motor for Isolated Grid Water Pump Application," *IEEE Transactions on Industry Applications*, vol. 56, no. 2, pp. 1907–1917, Mar. 2020, <https://doi.org/10.1109/TIA.2019.2959734>.
- [7] R. Chinthamalla, R. Karampuri, S. Jain, P. Sanjeevikumar, and F. Blaabjerg, "Dual Solar Photovoltaic Fed Three-Phase Open-End Winding Induction Motor Drive for Water Pumping System Application," *Electric Power Components and Systems*, vol. 46, no. 16–17, pp. 1896–1911, Oct. 2018, <https://doi.org/10.1080/15325008.2018.1520324>.
- [8] D. K. Dhaked and D. Birla, "Modeling and control of a solar-thermal dish-stirling coupled PMDC generator and battery based DC microgrid in the framework of the ENERGY NEXUS," *Energy Nexus*, vol. 5, Mar. 2022, Art. no. 100048, <https://doi.org/10.1016/j.nexus.2022.100048>.
- [9] A. Bughneda, M. Salem, A. Richelli, D. Ishak, and S. Alatai, "Review of Multilevel Inverters for PV Energy System Applications," *Energies*, vol. 14, no. 6, Jan. 2021, Art. no. 1585, <https://doi.org/10.3390/en14061585>.
- [10] M. Trabelsi, H. Vahedi, and H. Abu-Rub, "Review on Single-DC-Source Multilevel Inverters: Topologies, Challenges, Industrial Applications, and Recommendations," *IEEE Open Journal of the Industrial Electronics Society*, vol. 2, pp. 112–127, 2021, <https://doi.org/10.1109/OJIES.2021.3054666>.
- [11] A. Elgharbi, D. Mezghani, and A. Mami, "Intelligent Control of a Photovoltaic Pumping System," *Engineering, Technology & Applied Science Research*, vol. 9, no. 5, pp. 4689–4694, Oct. 2019, <https://doi.org/10.48084/etasr.2982>.
- [12] R. B. Bollipo, S. Mikkili, and P. K. Bonthagorla, "Hybrid, optimal, intelligent and classical PV MPPT techniques: A review," *CSEE Journal of Power and Energy Systems*, vol. 7, no. 1, pp. 9–33, Jan. 2021, <https://doi.org/10.17775/CSEEJPES.2019.02720>.
- [13] D. K. Dhaked, Y. Gopal, and D. Birla, "Battery Charging Optimization of Solar Energy based Telecom Sites in India," *Engineering, Technology & Applied Science Research*, vol. 9, no. 6, pp. 5041–5046, Dec. 2019, <https://doi.org/10.48084/etasr.3121>.
- [14] M. Y. Allani, D. Mezghani, F. Tadeo, and A. Mami, "FPGA Implementation of a Robust MPPT of a Photovoltaic System Using a Fuzzy Logic Controller Based on Incremental and Conductance Algorithm," *Engineering, Technology & Applied Science Research*, vol. 9, no. 4, pp. 4322–4328, Aug. 2019, <https://doi.org/10.48084/etasr.2771>.
- [15] B. Singh, U. Sharma, and S. Kumar, "Standalone Photovoltaic Water Pumping System Using Induction Motor Drive With Reduced Sensors," *IEEE Transactions on Industry Applications*, vol. 54, no. 4, pp. 3645–3655, Jul. 2018, <https://doi.org/10.1109/TIA.2018.2825285>.
- [16] K. Khan, S. Shukla, and B. Singh, "Performance Based Design of IMD for Single Stage PV Fed Water Pumping," in *2018 IEEE Industry Applications Society Annual Meeting (IAS)*, Portland, OR, USA, Sep. 2018, pp. 1–8, <https://doi.org/10.1109/IAS.2018.8544533>.
- [17] S. Shukla and B. Singh, "Single-Stage PV Array Fed Speed Sensorless Vector Control of Induction Motor Drive for Water Pumping," *IEEE Transactions on Industry Applications*, vol. 54, no. 4, pp. 3575–3585, Jul. 2018, <https://doi.org/10.1109/TIA.2018.2810263>.
- [18] A. Nouaiti, A. Saad, A. Mesbahi, M. Khafallah, and M. Reddak, "Design and Test of a New Three-Phase Multilevel Inverter for PV System Applications," *Engineering, Technology & Applied Science Research*, vol. 9, no. 1, pp. 3846–3851, Feb. 2019, <https://doi.org/10.48084/etasr.2573>.
- [19] X. H. Nguyen and M. P. Nguyen, "Mathematical modeling of photovoltaic cell/module/arrays with tags in Matlab/Simulink," *Environmental Systems Research*, vol. 4, no. 1, Dec. 2015, Art. no. 24, <https://doi.org/10.1186/s40068-015-0047-9>.
- [20] C. Boutahiri, A. Nouaiti, A. Bouazi, and A. M. Hsaini, "Experimental Test of a Three-Phase Inverter Using a Launchpad TMS320F28379D Card," in *Proceedings of the 3rd International Conference on Electronic Engineering and Renewable Energy Systems*, Saidia, Morocco, 2023, pp. 451–459, https://doi.org/10.1007/978-981-19-6223-3_49.
- [21] S. Murshid and B. Singh, "Single Stage Autonomous Solar Water Pumping System Using PMSM Drive," *IEEE Transactions on Industry Applications*, vol. 56, no. 4, pp. 3985–3994, Jul. 2020, <https://doi.org/10.1109/TIA.2020.2988429>.
- [22] Y. Aljarhizi, A. Nouaiti, E. A. Ibrahim, C. Boutahiri, A. Hassoune, and A. Mesbahi, "Optimized Wind Turbine Emulator based on an AC to DC Motor Generator Set," *Engineering, Technology & Applied Science Research*, vol. 13, no. 2, pp. 10559–10564, Apr. 2023, <https://doi.org/10.48084/etasr.5775>.
- [23] B. A. Nasir, "Determination of the Harmonic Losses in an Induction Motor Fed by an Inverter," *Engineering, Technology & Applied Science Research*, vol. 12, no. 6, pp. 9536–9545, Dec. 2022, <https://doi.org/10.48084/etasr.5012>.
- [24] C. Ramulu, P. Sanjeevikumar, R. Karampuri, S. Jain, A. H. Ertas, and V. Fedak, "A solar PV water pumping solution using a three-level cascaded inverter connected induction motor drive," *Engineering Science and Technology, an International Journal*, vol. 19, no. 4, pp. 1731–1741, Dec. 2016, <https://doi.org/10.1016/j.jestch.2016.08.019>.
- [25] S. Jain, A. K. Thopukara, R. Karampuri, and V. T. Somasekhara, "A Single-Stage Photovoltaic System for a Dual-Inverter-Fed Open-End Winding Induction Motor Drive for Pumping Applications," *IEEE Transactions on Power Electronics*, vol. 30, no. 9, pp. 4809–4818, Sep. 2015, <https://doi.org/10.1109/TPEL.2014.2365516>.